New Freckle Criterion for Technical Remelting Processes

B. Böttger[1)], G. J. Schmitz[1)], F-J. Wahlers[2)], J. Klöwer [2)], J. Tewes[2)], B. Gehrmann[2)]
[1] *Access, Aachen, Germany*
[2] *ThyssenKrupp VDM GmbH*
Corresponding author: e-mail b.boettger@access.rwth-aachen.de

Freckles present a serious type of defects in technical solidification processes like Electro Slag Remelting (ESR) or Vacuum Arc Remelting (VAR). They limit the maximum ingot size for many grades of steels and superalloys. Modelling of freckle formation thus is an important task for optimizing industrial remelting processes. Essentially, most freckle models published by now are based on a Rayleigh criterion. They are inspired by the classical concept that freckles are caused by an inversion of the liquid density in the semisolid region. Plumes of the lighter segregated liquid evolve through perturbation of the metastable layering of the melt in the mushy zone, a mechanism which motivates its description via a Rayleigh criterion. Such models, however, are not suitable in case of alloys which do not exhibit a liquid density inversion. These alloys should have a stable layering in the mushy zone and, accordingly, should not be prone to freckle formation. However, freckle formation is observed also in technical remelting processes of such alloys as a consequence of curved solidification fronts. The present paper describes a criterion which - instead of using a Rayleigh number - is based on the evaluation of the non-isothermal component of an instantaneous down-hill flow of heavy segregated melt in a melt pool with axial symmetry. Given the knowledge of the exact pool geometry and the shape and properties of the mushy zone, the occurrence of freckles can be predicted. A preferred initiation of freckles at mid radius is found for typical ESR pool profiles, without the need of assuming an anisotropic permeability of the mushy zone. The model equations are derived and discussed for simplified pool geometries. The new approach is compared to classical criteria, and implications for a better understanding of freckle formation in technical remelting processes are discussed.

Key words: freckle, ESR, VAR, alloy 718, downhill flow

Introduction

Due to their importance as a defect in alloy casting, freckles have been the subject of intense research efforts. They are in general considered to originate from convective instabilities during directional solidification, frequently also being denoted as chimneys [1,2], plumes [3,4], or channels [5-7].

A prerequisite for such convective instabilities is a liquid density inversion occurring when light elements are segregated into the interdendritic melt while a higher density melt is present at the dendrite tips [8,9].

Much work has been devoted to clarify the mechanisms underlying such convective instabilities, like e.g. in situ observation of plume and freckle formation in aqueous solutions [10] or in-situ x-ray investigations [11], and to control or suppress convective instabilities by means of e.g. external magnetic fields [12-15], vibrations [16], special nucleators [17], or dedicated alloy variations [52]. Fundamental investigations on convective instabilities during directional solidification of binary alloys [18-22] are complemented by numerical approaches [56] and experiments with forced convection/high gravity [23-25] and by numerous observations and results for superalloys and steels in view of their technical importance [26-35].

Many authors formulate a Rayleigh criterion in order to predict the onset conditions for convective

instabilities, e.g. [36,37]. Several of these approaches have also been extended for an inclined/tilted solidification front, e.g. [38,39].
With the assumption of different permeability values of the mushy zone [40,41] parallel and perpendicular to the dendrite growth direction, the preferential formation of freckles at the mid-radius of ESR ingot can be explained [42,32]. An instructive recent overview about a variety of freckle models for superalloys is given in [32].
Almost all present model scenarios are based on the formulation of a Rayleigh criterion relating buoyant driving forces for flow initialisation to stabilizing frictional forces. A mandatory pre-requisite for meaningfully applying such Rayleigh criteria thus is a density inversion being present in the liquid with a heavier - i.e. denser - liquid located on top of a lighter – less dense - liquid. Liquids with a stable layering, meaning a dense, heavy liquid at the bottom and a light liquid on the top, thus should not be prone to convection at all.
However, freckle type defects are also observed for alloy 718 in industrial castings [27,35,42,48,55], although heavy elements like Nb lead to an increasing density of the segregated melt during solidification of this alloy which should result in the formation of a stable layering. Similar to buoyancy driven freckles, these defects appear as dark spots in the cross-section, preferentially at mid-radius of the ingot. The freckle regions reveal a composition as observed in the strongly enriched interdendritic regions [8,44,45] and frequently consist of a chain of small equiaxed grains [44,51].
In the scientific discussion, this contradiction has not been addressed for long time. The lack of density inversion for alloy 718 was either ignored [44,35] or rejected, pointing out that the high silicon contents of older grades of alloy 718 could have led to a decreasing density of the melt during solidification [8,27,42].
Eventually, based on the study of longitudinal sections through alloy 718 ingots, the real nature of this defect could be described as a type of centre segregates [42] where heavy melt flows down along the pool surface. Due to the slight inclination of the channel with respect to the isotherm, the segregated melt gets in contact with already solidified material at higher temperature, and partial melting occurs.
Despite of these findings, Rayleigh number based criteria are still used to describe freckle initiation under those conditions [8,27,38,39,42,44], although the downhill flow of the heavy melt can be expected to be instantaneous, not requiring any initiation.
In the present paper, a new criterion for this type of channel segregates (“downflow freckles”) is developed. It complies with the more general definition of freckles as defects originating from flow-driven segregation caused by density differences of the melt inside the semi-solid zone. The freckle formation problem can thus be regarded as a case of thermo-solutal convection in a reactive porous medium [32]. Not only in case of a liquid density inversion, density differences can lead to a transport of highly segregated melt with lower temperature to regions of higher temperature, if the solidification front is tilted. Upon reheating, this segregated liquid can induce melting of the already solidified structures, thus widening the flow channel, and eventually breaking off dendrite arms which subsequently form new grains (Fig. 1).

Fig. 1: Flow balance in a differential volume element of the semisolid region (reprinted with kind permission from [48])

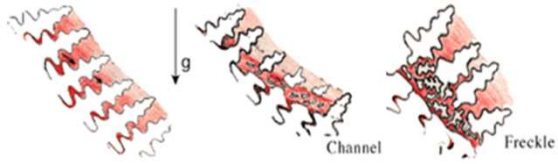

1. Development of a new freckle criterion

The important difference between downflow freckles and the classical case of a density inversion with upwards flowing plumes (buoyancy freckles) is the way how flow initiation occurs. For buoyancy freckles, at least if the solidification front is not tilted, there exists a priori no driving force for fluid flow (metastable situation). Considering a hypothetical cyclic flow path, the net force is 0 (Fig 2), and a perturbation of the liquid layers is necessary to initiate a cyclic flow (plume).
This is entirely different for alloys like alloy 718 when the solidification front is tilted. As can be seen in Fig. 3, there is a driving force for a cyclic flow pattern which is associated with an instantaneous downhill flow of the heavier melt in the mushy zone and an uphill flow of the lighter liquid above the solidification front. It is obvious that no specific criterion is needed for the onset of such kind of flow.

Fig. 2. Flow scheme for convection in case of a reduced interdendritic liquid density and a non-tilted solidification front (buoyancy freckles).

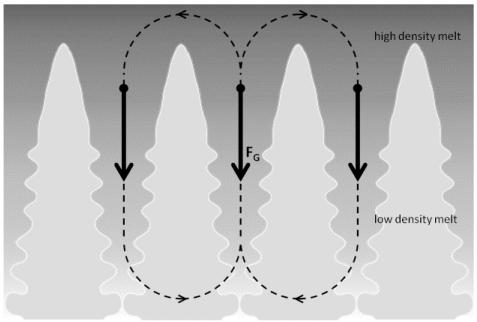

Fig. 3. Schematic representation of down-hill flow for high interdendritic liquid density and a tilted solidification front (downflow freckles).

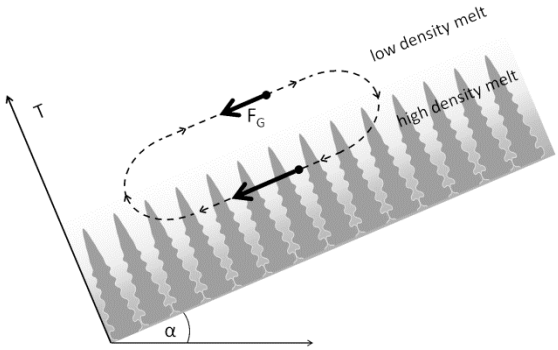

Once the existence of an instantaneous downhill flow is accepted, it is straightforward to define a criterion for freckle formation: As long as the flow essentially follows the isotherms, no melting will occur. But if for some reason – e.g. due to obstacles or due to a decreasing slope of the pool surface – the velocity of the downhill flow is reduced (Fig. 4), a flow component normal to the isotherms will arise. Melting of dendrite arms will occur if this perpendicular flow velocity exceeds the solidification velocity at this location (see below).

Fig. 4. Origin of a flow component $v_\perp$ perpendicular to the isotherms in a curved melt pool

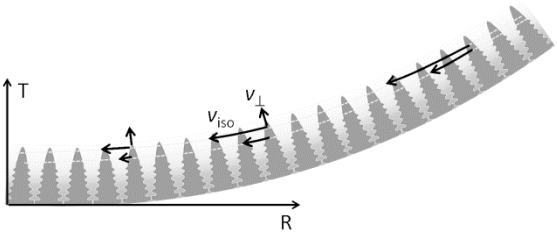

In the following it is assumed that, according to Darcy's law, the isothermal component of the downhill flow v_{iso} at temperature T can be described as a function of the density difference $\varrho(T) - \varrho(T_{Ref})$ with respect to the reference temperature T_{Ref} (temperature of dendrite tips), the temperature dependent permeability $K(T)$, and the inclination angle α as follows:

$$v_{iso} = -K(T)\frac{[\varrho(T)-\varrho(T_{Ref})]g}{\eta} sin\alpha \qquad (1)$$

with η being the kinematic viscosity of the melt, and g the gravity constant.
If a melt pool with axial symmetry is assumed, the non-isothermal flux component $v_\perp$can be derived considering a differential sector volume element with a thickness dT (Fig. 5) resp. dT/G, where G is the local temperature gradient.

Fig. 5. Flow balance in a differential volume element of the semisolid region

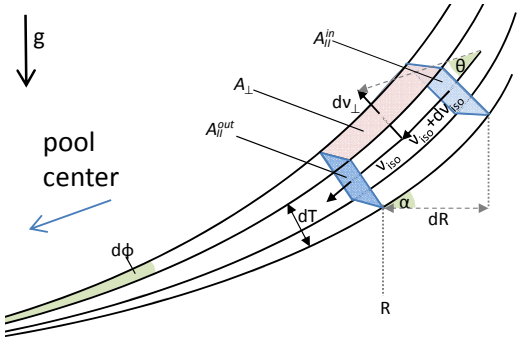

The differential flux change $dv_\perp$ can be obtained from the isothermal velocity change dv_{iso} and the cross sections $A_{//}^{out}$ and $A_{//}^{in}$ for the isothermal flow and $A_\perp$ for the non-isothermal flow component from continuity considerations:

$$A_\perp\, dv_\perp = A_{//}^{out}(v_{iso} + dv_{iso}) + A_{//}^{in} v_{iso} \qquad (2)$$

With equation (2) and:

$$A_{//}^{out} = \frac{d\varphi(\mathrm{R}+\mathrm{dR})}{2\pi}\frac{dT}{G+dG}, \qquad (3)$$

$$A_{//}^{in} = \frac{\mathrm{d}\varphi \mathrm{R}}{2\pi}\frac{dT}{G} \qquad (4)$$

and $$A_\perp = \frac{d\varphi \mathrm{R}}{2\pi}\frac{dR}{cos\,\alpha} \qquad (5)$$

the differential non-isothermal flux perpendicular to the temperature gradient can be calculated. $d\varphi$ represents the angular section of the rotationally symmetric pool profile (figure 5) and is not further important after inserting equations (3)-(5) into equation (2):

$$\mathrm{dv}_\perp = \frac{\mathrm{dT}}{\mathrm{RdR}}\left[\frac{(R+dR)(v_{iso}+dv_{iso})}{G+dG} + \frac{\mathrm{R}v_{\mathrm{iso}}}{\mathrm{G}}\right]\cos\alpha =$$

$$\frac{dT}{RdR}\left[\frac{v_{iso}R+v_{iso}dR+Rdv_{iso}+dv_{iso}dR}{(1+\frac{dG}{G})G} + \frac{\mathrm{R}v_{iso}}{G}\right] cos\,\alpha \qquad (6)$$

Assuming $dG \ll G$ and $dv_{iso}dR \ll v_{iso}R + v_{iso}dR + Rdv_{iso}$, we can replace equation (3) by

$$dv_\perp =$$

$$\frac{dT}{RdR}\left[(1-\frac{dG}{G})\frac{v_{iso}R+v_{iso}dR+Rdv_{iso}}{G} + \frac{\mathrm{R}v_{iso}}{G}\right] cos\,\alpha$$

$$= \frac{dT}{G}\left[-\frac{dGv_{iso}}{dRG} + \frac{v_{iso}}{R} + \frac{dv_{iso}}{dR}\right] cos\,\alpha \qquad (7)$$

Integration of $dv_\perp$ between the solidus temperature T_S and a given position in the mushy zone at temperature T* provides the value of the normal flow component at this position:

$$v_\perp(T^*, R) = \frac{1}{f_L(T^*)}\int_{T_S}^{T^*} f_L(T)dv_\perp =$$

$$\frac{1}{f_L(T^*)}\int_{T_S}^{T^*}\frac{f_L}{G}\left[-\frac{v_{iso}dG}{GdR} + \frac{v_{iso}}{R} + \frac{dv_{iso}}{dR}\right] cos\,\alpha\, dT \qquad (8)$$

This formulation for $v_\perp$, equation (8), comprises three contributions, equations (9), (10) and (11), which can be attributed to the effects of a variation of G, R and v_{iso} along the flow path:

$$v_{\perp,I}(T^*,R) = \frac{1}{f_L(T^*)}\int_{T_S}^{T^*}\frac{f_L}{G}\frac{dv_{iso}}{dR}\cos\alpha\, dT \qquad (9)$$

$$v_{\perp,II}(T^*,R) = \frac{1}{f_L(T^*)}\int_{T_S}^{T^*}\frac{f_L}{G}\frac{v_{iso}}{R}\cos\alpha\, dT \qquad (10)$$

$$v_{\perp,III}(T^*,R) = \frac{1}{f_L(T^*)}\int_{T_S}^{T^*}-\frac{f_L}{G}\frac{v_{iso}dG}{GdR}\cos\alpha\, dT \qquad (11)$$

Once the value of $v_\perp(T^*,R)$ is known all over the melt pool, a simple criterion for freckle formation can be derived according to Flemings [46]: If at any location through the mushy zone the local value of $v_\perp$ exceeds the local solidification velocity $\dot{T}/G_\perp$, freckle formation must be expected, as the upward flow of segregated melt in this case starts to dissolve dendrite arms or has a negative impact on the growth of the dendrite tips. As a consequence, the permeability of the mushy zone increases and the local flow pattern thus is further fostered.
The following sharp criterion for downflow freckle formation can thus be formulated:

$$C_F(R) = max\left(v_\perp(T^*,R)\frac{G_\perp(T^*,R)}{\dot{T}}\right) > 1 \qquad (12)$$

The maximum (max) here corresponds to the temperature T* in the mushy zone, where the maximum value of the argument is reached.
However, there is a further restriction for the maximum values of $v_\perp$: The effective flow direction, corresponding to a vector addition of the isothermal flow component v_{iso} and the non-isothermal flow component $v_\perp$, can never be directed upwards (i.e. $\vartheta < \alpha$, see Fig 6) as there is no driving force for the heavy melt to move against the gravity vector. This restriction is important close to the centre of the melt pool, where, due to the axial symmetry, the heavy melt is converging. Without this additional restriction, unphysical high values of $v_\perp$ would be predicted there. Instead, a lake of heavy melt is forming, and the flow direction is forced to be horizontal (Fig 6). As a consequence, the condition

$$v_\perp(T^*,R) < v_{iso}(T^*)\tan\alpha(T^*) \qquad (13)$$

has to be applied before calculating $C_F(R)$ according to Equation (12).

Fig. 6. Condition for "lake" formation

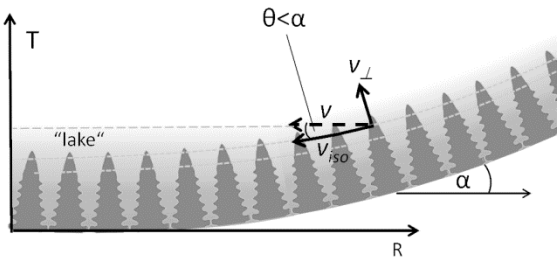

2. Parameter Study for a Model System for Alloy 718

The new freckle criterion for downflow freckles derived in Section 1 is a priori based on theoretical arguments. In contrary to classical Rayleigh number based criteria being typically calculated as function of the local tilt angle α and the local thermal gradient G, the new criterion depends on the local changes (derivatives) of α (Equation 9) and G (Equation 11). As a consequence, freckle prediction requires much more detailed knowledge about the actual shape of the pool profile and the individual isotherms, which is difficult to obtain experimentally.
For this reason the new criterion for downflow freckles is first applied to four hypothetical pool geometries, starting from a simple cone shaped profile and ending with a more realistic parabolic shape. The thermo-physical and process parameters, as given in Table 1 and Fig. 7, however, have been estimated close to a realistic electro-slag remelting (ESR) process of alloy 718 in order to allow for easy comparison to real technical processes.

Table 1. Material parameters used in this study

Parameter		**Estimated value**
liquidus temperature	T_{Liq}	1610°C
density of melt	$\varrho(T)$	7500 kg/m^3-10 (T-T_{Liq})
kinematic melt viscosity	η	0,008 kg/ms
primary dendrite spacing	λ_1	3 x 10^{-4} m
cross permeability (Blake-Kozeny)	K	$0.0649 + 0.0543\left[\frac{f_l}{1-f_l}\right]^{0.25}\lambda^2$ [2]
solidification velocity	$\dot{T}/G_\perp$	1.0 x 10^{-5}ms^{-1}

Fig. 7. Assumed fraction liquid-temperature curve

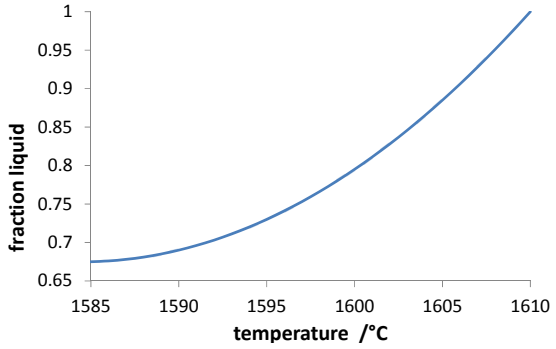

In the following, four different types of analytical pool profiles of a virtual ESR block of 0.5 m diameter are used to elucidate the general properties of the new downflow freckle criterion and to discuss the critical regions in the melt pool where freckle formation is to be expected. For evaluation of the new freckle criterion, explicit pool geometries are defined in form of the shape of individual isotherms. The four profiles with rotational symmetry being investigated in detail are (i) a simple cone shaped profile, (ii) a bi-conical profile, (iii) an elliptic profile, and (iv) a parabolic profile. Each of these profiles is characterized by a set of isotherms, which may locally vary with respect to their distance, i.e. the gradient. All three normal flow terms (Equations 9-11) which may contribute to freckle formation will be exploited successively using these dedicated profiles.

2.1. Cone Shaped Pool Profile

The cone shaped pool profile is characterized by isotherms with constant slope in the radial section and a constant distance between the isotherms. For the example in Fig. 8, the isotherms correspond to a constant temperature gradient of G=1054 K/m (normal to the isotherms) and a constant inclination of α=18.4°.

Fig. 8. Isotherms of a cone shaped pool profile corresponding to G=1054 K/m and α=18.4°.

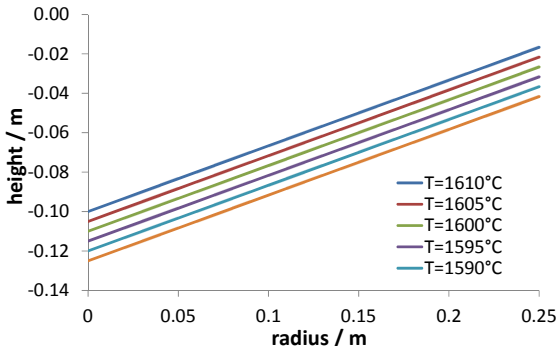

Fig. 9. Velocity profile through the mushy zone for the example of the cone shaped pool profile

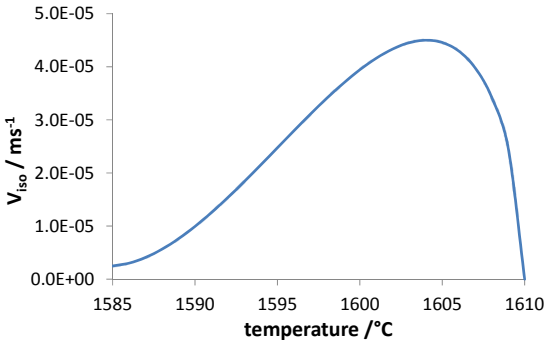

For each isotherm, an isothermal down-hill flow velocity v_{iso} is calculated (Equation 1). As can be seen in Fig. 9, the highest value of v_{iso} is found slightly below liquidus temperature where the value of f_L is about 85-90% (Fig. 7). As the normal flow terms (Equations 9-11) being responsible for freckle formation strongly depend on v_{iso}, it must be assumed that freckle initiation occurs in this region of high liquid fractions.

For conical pool profiles, the tilt angle α and the gradient G perpendicular to the isotherms are constant, and thus only term II of the normal flow velocity $v_\perp$ (Equation 10) is different from zero (Fig. 10). This term is due to the convergence of the isothermal flow in the cone shaped pool, and diverges in the centre of the pool for R=0.

Fig. 10. Term II of normal flow velocity $v_\perp$ (Equation 10). Terms I and III both are identical 0 in case of a cone shaped pool profile

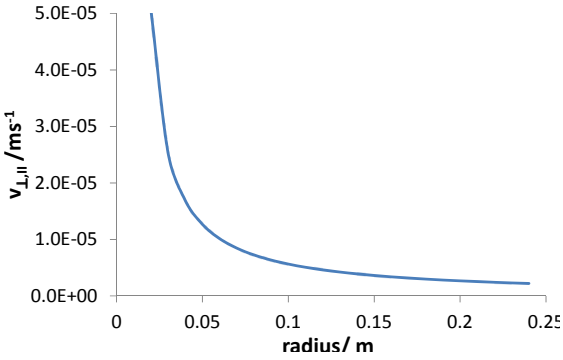

This divergence of term II of $v_\perp$ at r=0 would predict freckles at the pool centre for any pool geometry with radial symmetry if $v_\perp$ would not be limited by the fact that the total flow vector $\vec{v} = \vec{v}_\perp + \vec{v}_{iso}$ cannot be directed upwards without lake formation (Fig. 6, Equation 13). Nevertheless, for this geometry freckle formation is predicted close to the centre by Equations 12 and 13, as the criterion C_F exceeds a value of 1 for R<0.06 m (Fig. 11). Indeed, in V shaped melt pools, certain types of centre segregates ("V-segregates") can be observed [53], which are similar to freckles.

Fig. 11. Freckle criterion C_F (Equation 12) as function of the pool radius for the conical pool profile

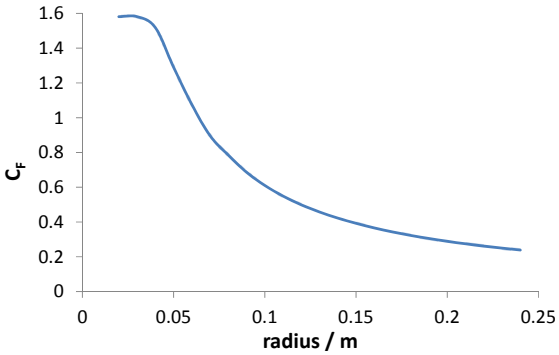

2.2. Biconical Pool Profile

The biconical melt pool profile, Fig. 12, is used as an example to demonstrate the effect of a step-like change in the tilt angle α. As a consequence, a step in the isothermal flow velocity v_{iso} arises. In order to obey the flux balance, a normal flux corresponding to a strong peak in term I (Equation 9, Fig. 13) must be present. Note that this peak is absent in the mere conical profile.

Fig. 12. Isotherms in the biconical pool profile (G_1=2022 K/m, α_1=8.4°, G_2=1159 K/m, α_2=26.6°).

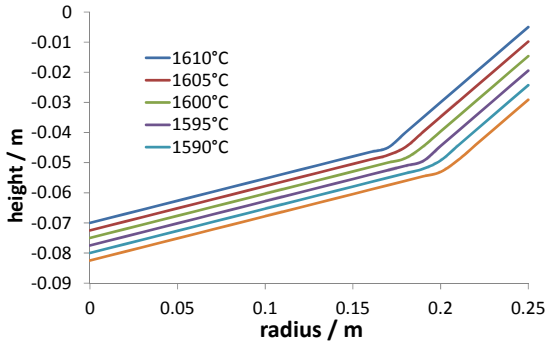

Fig. 13. Term I of normal flow velocity $v_\perp$ (Equation 9) for the biconical pool profile

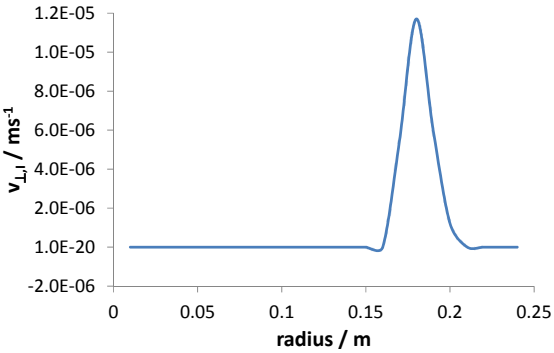

Fig. 14. Freckle criterion C_F (Equation 12) as function of the pool radius for the biconical pool profile

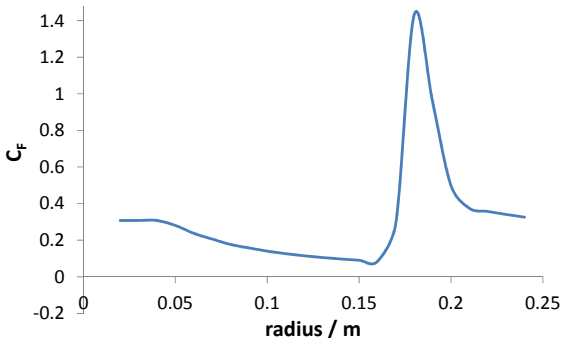

The peak in Fig. 13 dominates the shape of the overall freckle criterion curve (Fig. 14), and freckle formation is thus predicted around the radius of R~0.18m, where the step in the tilt angle α of the melt pool is located. Following the new freckle criterion, steps in the pool shape are critical and should thus be avoided.

2.3. Elliptic Pool Profile

In experimental melt pools, the tilt angle α of the isotherms and the thermal gradient G are typically varying simultaneously along the radius R of the pool. Thus, to obtain a realistic array of isotherms, ellipses of identical vertex and different co-vertices were combined as shown in Fig. 15.

Fig. 15. Isotherms in the elliptic pool profile $y(R,T)=-0.25+0.002\ (T-T_{Ref})\ [1-(4R)^2]^{1/2}$.

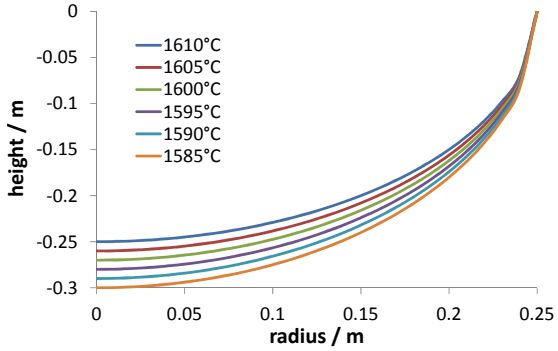

Fig. 16. Temperature gradient (at T=1604°C) for the elliptic pool profile

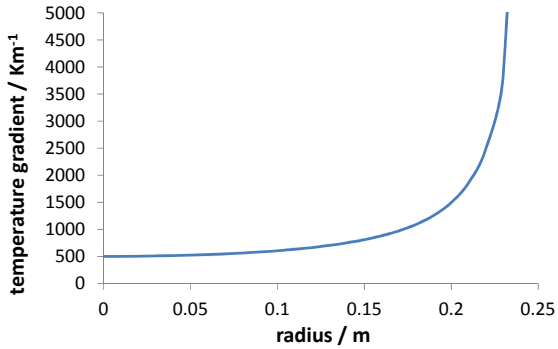

In the elliptic pool profile, the isotherms converge towards the edge of the pool (vertex of the ellipses). This corresponds to an increasing thermal gradient (normal to the isotherms), Fig. 16. On the other hand, the increasing tilt angle α leads to an almost linear increase of the isothermal downhill flow velocity v_{iso} , Fig. 17.

The effect of v_{iso} and G on the terms I-III of the normal flow velocity $v_\perp$ are summarized in Fig. 18. In term I, the linear increase of v_{iso} with R (Fig. 17) results in a constant positive value of dv_{iso}/dR. But the term also contains the factor f_S/G (Equation 9) which originates from the integration over the length of the mushy zone. Therefore, term I reveals a maximum at the pool centre and decreases to 0 towards the edge (Fig. 18).

Fig. 17. Downhill flow velocity profile at T=1604°C for the elliptic pool profile

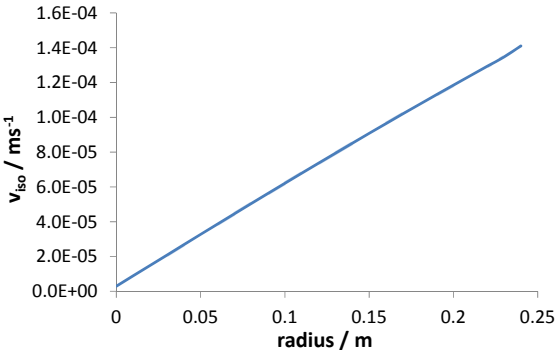

Term II has a very similar shape, as v_{iso}/R is also constant. Thus, terms I and II indicate an increased freckle risk close to the centre of the pool, while almost no risk is predicted for higher values of *R*. Term III, however, is negative for the entire range of *R*. This is due to the fact that the downhill melt flow, when going in direction towards the pool centre, experiences a decreasing thermal gradient and thus an increasing thickness of the mushy zone. For reasons of flux balance, liquid with a higher temperature is sucked down into the mushy zone. Therefore, a positive value of *dG/dR* is protective against freckle formation. In the case of the elliptic pool profile of Fig. 15, this protection is mainly effective at the pool edge, while at the pool centre *dG/dR* is about 0 (Figure 18).

Fig. 18. Terms I-III of the normal flow velocity $v_\perp$ (Equations 9-11) for the elliptic pool profile

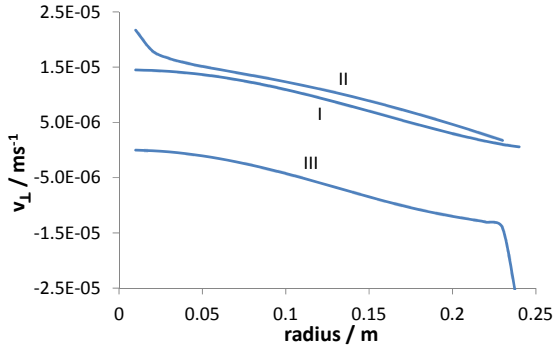

In summary, the combination of terms I-III would imply a high freckle risk especially at the pool centre. But the effect of "lake formation" (Equation 13) prevents freckling at this location if the pool centre is not very steep (like e.g. in case of the cone shaped profile in Fig. 8). Therefore, the freckle risk according to C_F (Fig. 19) increases to a maximum around *R*=0.1 m and decreases again towards the pool centre. In the radius range of about R=0,07-0,15 m, the value of C_F exceeds 1, indicating that freckling may be expected in this area.

Fig. 19. Freckle criterion C_F (Equation 12) as function of the pool radius for the elliptic pool profile

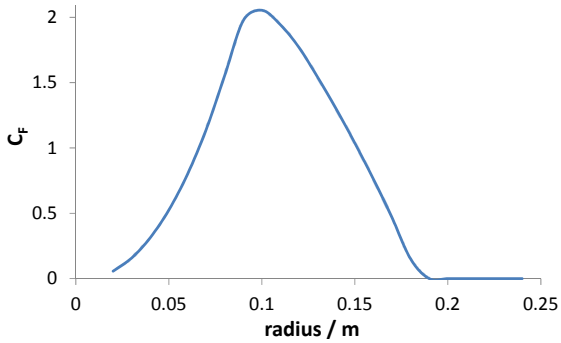

2.4. Parabolic Pool Profile

The parabolic pool profile, Fig. 20, is designed towards a flat shape around the centre and a maximum curvature at the edge. The properties of this pool profile with respect to term I-III of the normal flow velocity $v_\perp$ (Equations 9-11) are depicted in Fig. 21: The shape and relative position of the individual isotherms lead to a relative shifting of the effects of the tilt angle α and the the thermal gradient change *dG/dR*, both affecting $v_\perp$: While the positive (destabilizing) peak of term I is located around *R*=0.13 m, term III shows the strongest stabilizing effect (negative value) at *R*=0.17 m. The destabilizing term II originating from the radial convergence of the downhill flow, is considerably smaller but also reveals a maximum in this region. This is due to the fact that v_{iso} decreases towards the centre.

As a consequence, the freckle criterion C_F exhibits a strong and sharp maximum at around R=0.14 m (Fig. 22). This is close to the mid-radius position where freckles are most frequently detected in technical ESR processes. Fig. 21 further implies that the height of this maximum strongly depends on the exact shape of the isotherms as there are stabilizing and destabilizing contributions which partly mutually compensate. This fact emphasizes the necessity for an exact knowledge of the pool shape to correctly predict the tendency for freckle formation for a particular casting process.

Fig. 20. Isotherms in the parabolic pool profile $y(R,T)=0.25-0.002\ (T-T_{Ref})\ [(4R)^5-1)]$.

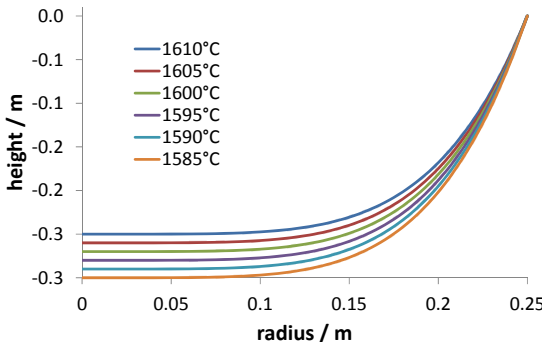

Fig. 21. Term I-III of normal flow velocity $v_\perp$ (Equations 9-11) for the parabolic pool profile

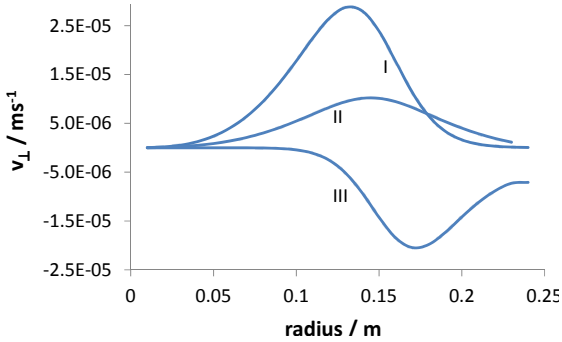

Fig. 22. Freckle criterion C_F (Equation 12) as function of the pool radius for the parabolic pool profile

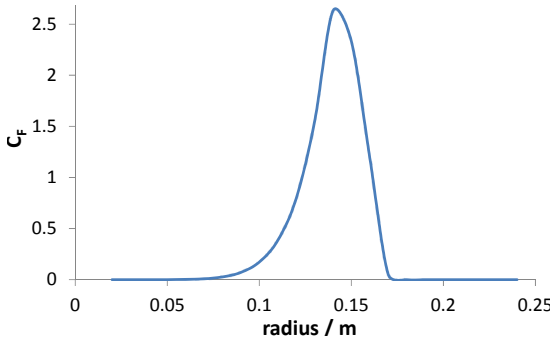

3. Discussion

The application of the newly developed freckle criterion to different model pool geometries has shown that this new criterion can be very helpful for understanding freckle formation in complex ESR or VAR remelting processes especially for alloys without liquid density inversion. Although by now no real, experimental pool profile has been examined, the results for the model pools appear reasonable. The new criterion provides an inherent tendency to predict freckles at intermediate radial positions, exactly where freckles are typically found in technical ingots. Furthermore, the criterion is sharply defined (C_F>1), thus not requiring any calibration.

Rayleigh number based criteria, in contrast, do not automatically show this tendency. To explain the preferred mid-radius position of freckles in ESR or VAR ingots, they require the assumption of an anisotropic permeability in the mush perpendicular resp. parallel to the growth direction [27,32]. Furthermore, an experimental calibration of the critical Rayleigh number is necessary which may even be not be identical for different types of alloys [47].

For these reasons, the use of Rayleigh number type criteria to predict freckle formation by now has been limited mainly to investment casting revealing an almost planar solidification front. Respective models seem to be less powerful in case of strongly curved pool profiles like in ESR or VAR [42].

Downflow freckles are expected to form at high liquid fractions (~85-90%) in the upper part of the mushy zone, i.e. close to the dendrite tips (see Fig. 8). The strong decrease of the permeability in the mushy zone for a liquid flowing perpendicular to the dendrite growth direction (.i.e. parallel to the isotherms) according to the Blake-Kozeny relation (Table 1) is the main reason for this conclusion. This seems to be in conflict with measurements of the freckle composition in alloy 718 implying that freckles are fed by a melt originating from a region in the mushy zone with a fraction liquid of about 0.4-0.6 [8,43]. However, it can be assumed that, even if freckles are initiated at considerably higher liquid fractions, they will erode the dendritic network, locally increase permeability, and thus penetrate downward deeper into the mushy zone. The initiation of classical buoyancy freckles at high f_L values has also been confirmed by numerical simulations [47].

Not only correct estimates for the permeability in the upper mushy zone, but also the knowledge of the exact dendrite geometry and the respective f_L-T relation are crucial. Such information cannot be obtained from simple solidification models. 3D microstructure simulation using e.g. phase-field models [49] need to be performed in order to obtain realistic values for the permeability and to estimate the liquid density distribution in the upper mushy zone.

Furthermore, the question arises whether the new understanding on downflow freckle formation presented in this paper might have as well implications for classical buoyancy freckles in ESR or VAR ingots. Even in case of an existing liquid density inversion, the argument of an instantaneous onset of fluid flow should still be valid. The resulting isothermal flow pattern, which in this case would be in uphill direction, could also lead to freckle formation or at least help to induce convective instabilities. Such an effect has been demonstrated by numerical simulation for a tilted casting and was interpreted in terms of a reduction of the critical Rayleigh number due to inclination [47].

Although the model equations, which have been derived in this paper for downflow freckles, are certainly not sufficient for prediction of the initiation of buoyancy freckles in curved pools, they could nevertheless at least indicate their preferential locations. Due to the opposite isothermal flow direction, the effects of Equations 9-11 would be reversed in case of a density inversion: For the parabolic pool profile of Fig. 21, term III would e.g. describe an increased freckle risk while terms II and III would stabilize the liquid layering. A freckle risk thus would be predicted close to the peak of term II at R=0.18 m. These relations indicate that the new approach presented in this paper may at least qualitatively explain also the mid-radius formation of classical buoyancy freckles in case of

strongly curved pool profiles.
Which could be the practical benefits to be drawn from the new approach? The classical criteria essentially rely on the principle of the highest local Rayleigh number. Various different definitions of the Rayleigh number have been published. There is some agreement that if a value of 0.22 [47] is exceeded, freckle formation can be expected. The exact and unique specification of a critical Rayleigh number, whether being the length of the mush or the thermal diffusion length, is a further an open issue in this context [36].
Even disregarding the exact formulation of the Rayleigh number and criterion, the practical implications of such models are limited: The use of high thermal gradients as well as high melting rates should decrease the freckle risk in ESR. This is well-known, but hard to be realized in practice when producing large diameter ingots. Actual Rayleigh models also predict an increasing risk of freckle formation with an inclination of the solidification front, but the exploitation of this knowledge to optimise processes involving complex shaped melt pools has not been successful by now.
In this situation, the new approach could be much more promising. With respect to freckle formation in large ingots of alloys without liquid density inversion like alloy 718 – and this is where the proposed approach is essentially aiming at – the new freckle criterion offers new directions not only for the understanding of the nature of freckles, but also with respect to the possibilities of their prevention/suppression.
One consequence of the model equations is that, without any inclination, freckle formation should be impossible at any local Rayleigh number, as long as the liquid density is increasing with decreasing temperature in a "stable layering". This is evident as all three contributions to a possible non-isothermal flow $v_\perp$(Equation 9-11) vanish if v_{iso} is zero. But the pool shape should not only be as flat as possible: In contrast to the classical criteria, the change of inclination, i.e. the curvature of the pool profile or more exactly $dcos(\alpha)/dR$, is essential and should be reduced in order to minimize term I of $v_\perp$(Equation 9). At the same time, according to Equation 11, an increasing gradient along the pool radius can help to avoid freckles, if this increase is located appropriately.
Of course, these parameters cannot be selected independently as they are interrelated and determined by the process parameters. By using process simulation [50] it should be possible to monitor the influence of these parameters on the pool shape and, with the help of the new freckle criterion, on the predicted freckle risk. The strong influence of the exact shape of the isotherms on the balance between the three terms of $v_\perp$ has been clearly demonstrated in the present paper on the basis of simple model pool geometries.
As a possible extension of this model, macroscopic flow pattern due to thermal convection [54] or induction could be included by adding the local velocity values to v_{iso}. The result would be a locally increased or decreased risk for freckle formation, depending on the macroscopic flow direction. Further possible extensions relate to the consideration of contributions to $v_\perp$ originating from flow evoked by density discontinuities between solid and liquid.

Conclusions and Outlook

An entirely new approach to freckle formation during ESR or VAR of alloys without liquid density inversion like alloy 718 has been developed. Unlike in most classical freckle criteria, no Rayleigh number is used. Instead, the present approach is based on the evaluation of the non-isothermal component of an instantaneous flow of heavy melt down towards the centre of the melt pool. This new approach allows for the definition of a sharp criterion for freckle formation which is based on the pool shape (geometry of the isotherms), the density gradient in the melt, the permeability of the mushy zone and the solidification rate.
Although up to now no real industrial remelting process has been examined, the application to model pool geometries already led to promising results. A strong tendency of the model to predict freckles in the mid-radius position of the pool has been elaborated and it could be shown that the results strongly depend on the exact shape of the pool geometry.
For further validation, the criterion has to be applied to a realistic remelting process and respective pool geometries. Future work will thus draw on process simulations allowing determining exact pool geometries for industrial ESR processes. Additionally, 3D microstructure simulation of the upper mushy zone using the phase-field method will be performed [49] in order to exactly evaluate the permeability as a function of temperature. Based on respective findings possible modifications of the process parameters will we exploited in view of reducing the risk of freckle formation in industrial remelting processes.

References

1. Chung C.A; Worster M.G.: Journal of Fluid Mechanics 455 (2002) 387
2. Loper D.E.; Roberts P.H.: Studies in Appl. Math. 106 2 (2001) 187
3. Chung C.A.; Chen F.L.: Journal of Fluid Mechanics 408 (2000) pp. 53-82
4. Nishimura T.; Sasaki J.; Moo T.T.: Int. J. of Heat and Mass Trans. 46 23 (2003) pp. 4489-4497
5. Frueh C. et al.: Materials Science and Engineering A 345 1 (2003) 72
6. Hellawell A.: Crystal Properties and Preparation 22-25 1 (1989) 347

7. Jain J.; Kumar A.; Dutta P.: J. of Heat Transfer- ASME 129 4 (2007) 548
8. Auburtin P.; Cockcroft S.L.; Mitchell A.: Superalloys 1996 pp 443-450
9. Copley S.M. et al.: Metallurgical Transactions 1 8 (1970) 2193
10. Tan F.L.; Tso C.P.; Pek P.K.: Int. Comm. in Heat and Mass Transfer 30 8 (2003) 1101
11. Boden S.; Eckert S.; Gerbeth G.: Materials Letters 64 12 (2010) 1340
12. Bergman M.I.; Fearn D.R.; Bloxham J.: Metall. Mater. Trans. A 307 (1999) 1809
13. Ebisu Y.: Metallurgical and Materials Transactions B 42 2 (2011) 341
14. Medina M.; Du Terrail Y.; Durand F.; Fautrelle Y.: Metall. Mater. Trans. B 35 4 (2004) 743
15. Muddamallappa M.S.; Bhatta D.; Riahi D.N.: Transport in Porous Media 79 2 (2009) 301
16. Govender S.: Transport in Porous Media 88 2 (2011) 225
17. Shafii M.B.; Dehkordi E.A.; Moghadam M.E.; Koochesfahani M.M.: Exp. Thermal and Fluid Sci. 33 8 (2009) pp. 1209-1215
18. Fowler A.C.: IAM Journal of Appl. Mathematics 35 2 (1985) 159
19. Amberg G.; Homsy. G.M.: Journal of Fluid Mechanics 252 (1993) 79
20. Garimella S.V.; McNulty J.P.; Schlitz L.Z.: Metallurgical and Materials Transactions A 26 4 (1995) 971
21. Felicelli S.D.; Heinrich J.C.; Poirier D.R.: J. Cryst. Growth 191 4 (1998) 879
22. Frueh C.; Poirier D.R.; Felicelli S.D.: Materials Science and Engineering A 328 2 (2002) 245
23. Riahi D.N.:J. Cryst. Growth 226 3 (2001) 393
24. Neislon D.G.; Incropera F.P.: Int. J. of Heat and Mass Trans. 36 2 (1993) 489
25. Quillet G. et al.: Modeling of Casting, Welding and Advanced Solidification Prosesses X (2003) 253
26. Wang L.; Zhong B.Y.; Dong J.X.; Zhang M.C.: Rare Metal Materials and Engineering 36 12 (2007) pp. 2104-2108
27. Auburtin P.; Wang T.; Cockcroft S.L.; Mitchell A.: Metall. Mater. Trans. B 31 4 (2000) 801
28. Gu J.P.; Beckermann C.; Giamei A.F.: Metall. Mater. Trans. A 28 7 (1997) 1533
29. Wlodeck S.T.; Field R.D.: Superalloys 718, 625, 706 and various derivatives (1994) pp. 167-176
30. Schneider M.C. et al.: Metall. Mater. Trans. A 28 7 (1997) 1517
31. Cao H.F.; Shen H.F.; Liu B.C.: Rare Metal Materials and Engineering 35 12 (2006) 1849
32. Valdes J.; King P.; Liu X.B.: Metall. Mater. Trans. A 41 A 9 (2010) 2408
33. Tin S.; Pollock T.M.: Journal of Materials Science 39 24 (2004) pp. 7199-7205
34. Long Z.D.; Yang W.H.; Chang K.M.: Superalloys 718, 625, 706 and various derivatives (2001) pp. 745-754
35. Morita K.; Suzuki T.; Taketsuru T.; Evans D.G.; Yang W.: Superalloys 718, 625, 706 and various derivatives (2001) pp. 149-160
36. Ramirez J.C.; Beckermann C.: Metall. Mater. Trans. A 34A 7 (2003) 1525
37. Yang W.H. et al.: Metall. Mater. Trans. A 322 (2001) pp. 397-406
38. Yang W.H. et al.: JOM 56 9 (2004) pp. 56-61
39. Baker C.F.; Riahi D.N.: Centrifugal Materials Processing (1997) pp. 163-168
40. Erdmann R.G.; Porier D.R.; Hendrick A.G.: Materials Science Forum 649 (2010) pp. 399 408
41. Poirier D.R.: Met Trans B 18 1 (1987) 245
42. Auburtin P.; Cockcroft S.L.; Mitchell A.; Schmalz A.J.: Superalloys 718, 625, 706 and Various Derivatives, TMS (1997) 47
43. Madison J. et al.: Metall. Mater. Trans. A, 43A (2012) 369
44. Yang W.H. et al.: Superalloys 718, 625, 706 and various derivatives (2001) 113
45. Yu K.O. et al.: Journal of Metals 1 (1986).46
46. Flemings M.C. and Nereo G.E.: Trans TMS-AIME 239(1967) pp. 1449-61.
47. Beckermann C.; Gu J.P. and Boettinger W.J: Metall. Mater. Trans. A, 31A (2000) 2545.
48. Van den Avyle J.A., Brooks J.A., Powell A.C.: JOM 50 3 (1998) 22
49. www.micress.de (accessed 05/2012)
50. Giesselmann N.; Rückert A.; Pfeifer H.: SteelSim 2011, 4th International Conference on Modelling and Simulation of Metallurgical Processes in Steelmaking, 27. Juni - 1. Juli 2011, Düsseldorf
51. Giamei A.F.; Kear B.H.: Metallurgical Transactions 1 8 (1970) 2185
52. Rösler J. et al.: Advanced Engineering Materials 5 7 (2003) 469
53. Mehrabian R.; Keane M.; Flemings M.C.: Met. Trans. 1 (1970) 2009
54. Sahai V.; Overfelt R.A.; Banerjee P.: Superalloys 718, 625, 706 and various derivatives (1996) 107
55. Kennedy R. et al.: Advanced Technologies for Superalloy affordability TMS (2000) 159
56. Felicelli S.D.; Poirier D.R.; Heinrich J.C.: Metall. Mater. Trans. B 29 4 (1998) 847